Metal casting into NaCl molds fabricated by material extrusion 3D printing

René Wick-Joliat[1] · Dirk Penner[1]

Abstract

Aluminum die casting is a well-established industrial process for mass producing aluminum parts with complex shapes, but design restrictions exclude some features like undercuts and hollow structures from being produced with this method. Water-soluble casting molds offer a promising solution to overcome those restrains, for example by hot pressing of salt cores or 3D printing of NaCl molds. Presently, 3D printing techniques available for NaCl are limited to direct ink writing (DIW) and photopolymerization. This study presents an approach to prepare NaCl parts by thermoplastic material extrusion (MEX) 3D printing. Firstly, a 3D printable feedstock is developed consisting of an organic binder, which is usually used for ceramic injection molding, and sodium chloride (NaCl) salt crystals. Various molds are then printed on a granulate-fed MEX printer. After thermal debinding and sintering at 690 °C, the 3D printed parts consist of pure NaCl. Furthermore, the same NaCl feedstock is used for injection molding. The bending strength of 3D printed samples with and without post-treatment are measured and compared to injection molded test specimens. Finally, metal casting in 3D printed NaCl molds is shown with tin or aluminum and the metal demonstrator parts with complex geometries such as gyroid structures and turbine wheels are released by dissolving the NaCl molds in water.

1 Introduction

Aluminum die casting is a widespread method for producing large numbers of complex parts such as engine blocks. Thanks to its short cycle time (few seconds up to 1 min) and the ability for casting thin walls it has high potential for lightweight design [1, 2]. However, due to increasing requirements for higher functionality and integrating hollow channels for diverse media such as water, oil and air into the Al parts, the die casting molds become increasingly complex. Salt cores are therefore used for casting cavities, holes and undercuts and dissolved after casting [3]. These salt cores are conventionally produced through pressing or casting of molten NaCl. [4–6] Recently, NaCl parts have been prepared by additive manufacturing. Kleger et al. have utilized direct ink writing (DIW) to 3D print NaCl

structures, which were subsequently sintered, infiltrated with molten magnesium, and ultimately dissolved to yield a Mg scaffold [7]. Similarly, Gong et al. reported DIW of salt cores from NaCl/Na$_2$SO$_4$/bauxite slurries. By adding up to 30 wt% of bauxite to the slurry, they were able to increase the bending strength of the sintered samples at the expense of a decreased water-solubility rate [8]. However, the parts presented in the two DIW studies had geometries with limited complexity and showed deformation during drying and sintering.

In a subsequent work, Kleger et al. reported a vat photopolymerization-based approach for 3D printing NaCl molds. These molds were employed in the casting of silicone, poly(DLLA-co-CL), aluminum, and chocolate [9]. Alternatively, Gallien et al. have used an indirect method by 3D printing periodic cellular structures from PLA which were then used to produce NaCl molds. After sintering and pyrolysis of the PLA, the sacrificial NaCl molds were used for aluminum casting [10].

Sacrificial molds may also be printed from water-soluble polymers [11–14]. Those molds are limited in their application for conventional metal casting due to their melting

✉ René Wick-Joliat
  rene.wick@zhaw.ch

1 Institute of Materials and Process Engineering, ZHAW Zürcher Hochschule für Angewandte Wissenschaften, Technikumstrasse 9, 8401 Winterthur, Switzerland

temperatures which are lower than the casting temperatures of most commercially important metals. NaCl combines the advantages of high solubility in water with a high melting point of 801 °C, which is higher than the casting temperature of aluminum.

In the present study, we introduce a novel method for creating water-soluble NaCl molds using thermoplastic material extrusion (MEX) 3D printing. MEX is a widely recognized technique for printing objects from thermoplastic materials. Thanks to its low setup and running costs and user-friendly operation and feedstock handling (as compared to other 3D techniques such as photopolymerization and DIW), MEX is widely used by professionals and hobbyists alike. Two commonly used material feeding methods are filament and granulate. Filament spools have been the traditional choice for most 3D printers due to their superior printing quality [15, 16]. But in recent years, granulated materials have emerged as an alternative option owing to their affordability and availability in large quantities (> tons) [17, 18]. It is noteworthy that some materials, such as very soft or highly filled materials, pose significant challenges in converting them into filaments. To make metals and ceramics printable through MEX, a thermoplastic binder is blended with a significant amount of solid filler, typically exceeding 40 vol% of ceramic or metallic powder [19–27]. The high filling of the feedstock leads to additional challenges during printing, for example difficulties to print overhangs and bridges, layer-to-layer adhesion or clogging of the nozzle. However, through careful selection of the binder components and print settings, the achieved printing qualities are comparable to unfilled thermoplastic materials. The printed ceramic or metallic object, referred to as a "green body," undergoes a process of thermal debinding and sintering, during which the metallic or ceramic object densifies and shrinks, ultimately resulting in the final part.

The NaCl feedstock presented in this work consists of NaCl and a thermoplastic binder system, typically utilized for ceramic injection molding (CIM). The use of a commercially available CIM binder system confers numerous advantages, including the availability of the material in large quantities at a reasonable cost, and established debinding procedures (either thermally or through the use of a solvent). Additionally, as the majority of the requirements for a CIM feedstock overlap with those of a MEX 3D printing feedstock, scaling up from prototyping via 3D printing to industrial production through CIM can be accomplished quickly and efficiently. The NaCl feedstock described herein has been formulated by Wick-Joliat and Penner as a supporting material for multimaterial ceramic MEX [28] and uses the Embemould K83 binder system. The same binder was previously employed in the creation of a library of ceramic feedstocks derived from Al_2O_3, ZrO_2, and $MoSi_2$ composites for MEX [24, 29]. Here, we show the printing and sintering

behavior of NaCl parts and demonstrate a way to increase the surface smoothness by immersion of printed or sintered parts into saturated NaCl solution. Additionally, we report injection molding of NaCl parts from the same feedstock used for 3D printing. This method is especially interesting for the aluminum die casting industry as it is capable of rapidly producing large numbers of salt cores. By allowing the same feedstock to be used for both MEX and injection molding, a simple transfer from rapid prototyping to industrial mass production is possible. Next, the bending strength of sintered samples with and without post-treatment is investigated and finally, metal casting is presented on tin and aluminum.

2 Materials and methods

2.1 Materials

NaCl (99.5%, Sigma-Aldrich) was ground in a Nutri Bullet 600 blender and particles below 100 μm were obtained by sieving and further used for feedstock preparation. Embemould K83, the binder system, was purchased from Krahn Ceramics and LDPE (LD 655) from ExxonMobil. Tin soldering wire TSC Kristall 400 was produced by Stannol, Germany. The aluminum alloy used for casting was Silafont-36 (AlSi10MnMg).

2.2 Feedstock preparation

The NaCl feedstock was prepared by manually mixing NaCl powder (< 100 μm particle size), Embemould K83 and LDPE combined in the weight ratio 80:19.2:0.8 and fed into a twin screw extruder (ZE 18 HMI, Three-Tec, Switzerland) and extruded at 130 °C through a 2 mm nozzle. The extruded filament was crushed into smaller pieces and fed into the extruder again. This cycle was repeated five times to ensure sufficient homogeneity. Finally, the feedstock was granulated in a Nutri Bullet 600 blender and the particles with sizes of 200–500 μm were collected for 3D printing by sieving.

2.3 Feedstock characterization (rheology, TGA, DSC)

The Embemould binder system was analyzed by differential scanning calorimetry (DSC) on a DSC 204 F1 Phoenix (Netzsch, Germany). A nitrogen gas flow was set to 40 ml/min and the samples were heated in aluminum pans with pierced caps from – 80 to 180 °C (20 °C/min). After cooling down to – 80 °C at 10 °C/min, a second heating cycle to 180 °C was recorded and only this second heating was used for DSC analysis.

The rheological measurements of the Embemould binder were carried out on an MCR301 rheometer (Anton-Paar,

Austria) equipped with a CTD 450 heating chamber. A plate–plate geometry with 25 mm diameter was used in oscillation mode. The static force was set to 0.25 N, the deformation to 0.1%, and the angular frequency was swept from 0.1 to 50 rad/s. An angular frequency sweep was done in 10 °C steps between 80 and 180 °C after a temperature equilibration time of 5 min at each temperature step.

To determine the softening point of the feedstock, penetration tests were carried out using a Q 800 dynamic mechanical analysis (DMA) instrument (TA Instruments, Germany). The penetration accessory was utilized for the cantilever clamp. During the measurement, a static force of 1 N was exerted to the penetration tip, which was mounted to the dynamic portion of the clamp. The feedstock samples were approximately 1 mm in thickness and 5 mm in diameter, and were placed in the sample holder located at the static part of the clamp. The setup was heated at a rate of 3 °C/min from 30 to 150 °C, and the softening point was determined as the temperature at which the tip fully penetrated the feedstock sample.

Thermogravimetric analysis (TGA) measurements were performed on a Netzsch 449 C Jupiter instrument between 20 and 800 °C at either 1 or 5 °C/min. The analyzed specimens were 3D printed cubes of roughly $4 \times 4 \times 4$ mm.

The shrinkage of printed parts during debinding and sintering was observed by an optical dilatometer (L74HS1600, Linseis, Germany). The sample was heated in air at a constant rate of 1 °C/min from room temperature to 690 °C with a dwell time of 1 h before cooling down to room temperature with 2 °C/min.

2.4 Printing

All parts were printed on a 3D printer constructed in our research group and outfitted with two granulate-feed extrusion units [29]. The extrusion units are attached to a frame that moves in the z-direction, while the printing bed moves in the x- and y-directions. The print heads are affixed to a linear guide, which allows for the inactive head to be lifted a few millimeters by a servomotor. The granulate is stored in a funnel reservoir. The extruder features three temperature zones: an air-cooled zone at the granulate inlet, a pre-heating zone, and the main heating zone with an interchangeable nozzle. The print bed is covered with a textured PEI sheet and the maximum build size is $180 \times 150 \times 150$ mm. The printer is controlled by a Duet 2 wifi board, and slicing is accomplished in Simplify 3D software. All printed parts were designed using Autodesk Fusion 360.

High printing quality with the NaCl feedstock was achieved with the following printing parameters: Nozzle temperature 130 °C, pre-heating zone 70 °C, printing bed 70 °C. Most parts shown in this study were printed with a 0.6 mm nozzle and 0.3 mm layer height. As an exception,

the turbine mold was printed in two parts with different settings: the bottom part holding the turbine was printed with a 0.4 mm nozzle and 0.2 mm layer height, while the top part consisting of the lid and the funnel for metal casting was printed with a 0.8 mm nozzle and 0.4 mm layer height to save some printing time. The line width was set to the standard value of 120% of the nozzle diameter (0.72 mm for 0.6 mm nozzle) and most prints were performed with two perimeter lines, three top and bottom layers and an infill density of 50% and rectilinear infill geometry with alternating +45°/-45° printing direction.

2.5 Injection molding

A BOY XS machine was used for injection molding rectangular rods ($80 \times 10 \times 4$ mm) from the same NaCl feedstock used for 3D printing. Temperatures were set to 150, 140, 130 °C for nozzle, intermediate, and barrel temperature. The tool was heated to 50 °C. Molding was performed at 150 bar with 60 bar holding pressure and 15 s of cooling before demolding. With those settings, 30 bars were molded in full automation mode.

2.6 Debinding/sintering

Thermal debinding and sintering was done in a box furnace LHT 02/18 or 04/18 (Nabertherm, Germany). The temperature was increased from room temperature to 500 °C at a rate of 20 °C/h for large parts and 50 °C/h for smaller parts. After a dwell time of 2 h, temperature was increased to the final sintering temperature of 690 °C (except for some sintering tests at 710 or 730 °C as mentioned in the text) with a dwell time of 2 h.

Injection molded samples were debound and presintered in an Al_2O_3 powder bed at 650 °C with 50 °C/h heating rate and 1 h dwell time. The powder bed was necessary to avoid bloating of the samples. Sintering was performed with the same procedure as for 3D printed parts.

2.7 Post-treatment, bending tests

For the post-processing and bending tests, rectangular rods of $4 \times 3.5 \times 50$ mm were printed with 100% infill but without perimeter lines. The infill direction was along the length of the rods. Eight samples were sintered without post-treatment, eight samples were immersed in an aqueous solution of saturated NaCl before sintering, and an additional eight samples were sintered and then immersed in NaCl solution. After NaCl immersion, samples were blown dry in a stream of pressurized air. Three point bending tests were conducted at room temperature on a Zwick Z010 mechanical testing machine. Testing width was set to 40 mm and displacement speed was

0.02 mm/s. Bending strengths were calculated as average values of four samples.

2.8 Characterization (optical microscopy, SEM)

Scanning electron microscopy was performed on a Phenom XL Desktop (Thermo Fisher Scientific) and a VHX 6000 (Keyence) was used for light microscopy.

2.9 Tin casting

All molds were designed by CAD in Fusion 360 or Blender software by subtracting the target geometry from a bigger body and adding an inlet with funnel as well as some outlet for air to escape. The outer wall of the mold was designed with a minimum thickness of two printing lines, corresponding to 1.44 mm for molds printed with a 0.6 mm nozzle and 0.96 mm for the 0.4 mm nozzle. The small molds for the gear and cubane structure were printed as one body, while the larger and more complex molds for the gyroid cube and the turbine wheel were split into a bottom part holding the mold and a top part with the inlet. The two parts were then combined by coating the interface with NaCl solution and drying the mold at 40 °C.

A solder wire with the composition Sn95.5/Ag3.8/Cu0.7 (TSC Kristall 400, melting temperature 217 °C, Stannol, Wuppertal) was used for tin casting. To remove the flux, the solder wire was first heated in a crucible with a heat gun. The molten solder was then poured into cold water to separate the metal from the flux. The NaCl mold and the tin in a crucible were heated in a furnace to 250 °C. Alternatively, the tin was molten in an Al_2O_3 crucible by a hot air gun. The tin was then poured into the mold and allowed to cool down to room temperature. Subsequently, the NaCl mold was dissolved by immersion into a beaker filled with water.

2.10 Aluminum casting

The NaCl molds were placed inside a larger Al_2O_3 crucible and the interspace was filled with Al_2O_3 powder. A large enough piece of Al was placed in a porcelain crucible. The crucible with the NaCl mold and the crucible with the Al were then heated to 710 °C in a bottom loader furnace (Carbolite Gero). After 30 min at 710 °C, the furnace was opened and the molten Al poured into the NaCl mold. An Al_2O_3 pistil was used to further press the liquid metal into the mold. After cooling the filled mold to room temperature, the NaCl was dissolved in water.

3 Results and discussion

Firstly, a NaCl feedstock was developed using a commercially available CIM binder system. The same binder system was previously used for multiple ceramic MEX printing feedstocks [24, 28].

Formulations with solid loads of 53, 61 and 67 vol% NaCl were investigated and the feedstock with the highest solid load showed the most reliable printing quality, while occasional powder-binder demixing was observed for the feedstock containing 53 vol% NaCl [28]. Generally, high solid loads are preferable because the lower shrinkage typically leads to better dimensional accuracy and less deformations. However, feedstocks with NaCl contents above 70 vol% were not printable due to their high viscosity. For those reasons, all results presented herein were obtained from feedstocks with 67 vol% NaCl. The particle size of commercial NaCl powder was up to 500 μm which is too big for MEX 3D printing with nozzles of 0.4–0.8 mm. Therefore, NaCl powder was crushed and sieved with a 125 μm sieve. Due to low hardness of NaCl and high shear stresses during feedstock preparation the particles in the finished feedstock were even smaller. Commercial CIM binder systems consist of at least four components. The backbone binder with a high molecular weight is responsible for structural strength, a lubricant with lower molecular weight ensures good flowability and is often soluble in water or other solvents to facilitate the debinding step. Surfactants serve as a link between ceramic particles and the binder and a plasticizer increases the plasticity and decreases viscosity [30]. DSC confirmed that the binder system Embemould K83 contained four different components, the first of which was melting at 65 °C (Fig. 1A). Due to the melting of a major component, the feedstock abruptly turned from hard and brittle into soft and slightly sticky around 65 °C. As an implication of this change, rotational rheology was possible at temperatures above this first melting point, since the sample pellets would now stick to the test setup. Two other components melted at 110 °C and 157 °C, and both melting points were associated with a viscosity decrease of almost two orders of magnitude (Fig. 1A). Between 110 and 150 °C, the viscosity was around 100 Pa·s which was ideal for 3D printing. An advantage of the high solid load of 67 vol% was the increased green body strength as compared to feedstocks with only 53 vol% or 60 vol%. This was reflected in penetration tests during which a constant force of 1 N was applied to a metal tip and pressed against a feedstock pellet (Fig. 1B). At 53 vol% NaCl the tip penetrated the sample at 57 °C, which was lower than the melting point of the first binder component. The feedstock pellet with 67 vol% NaCl was only penetrated at 79 °C due to its higher green
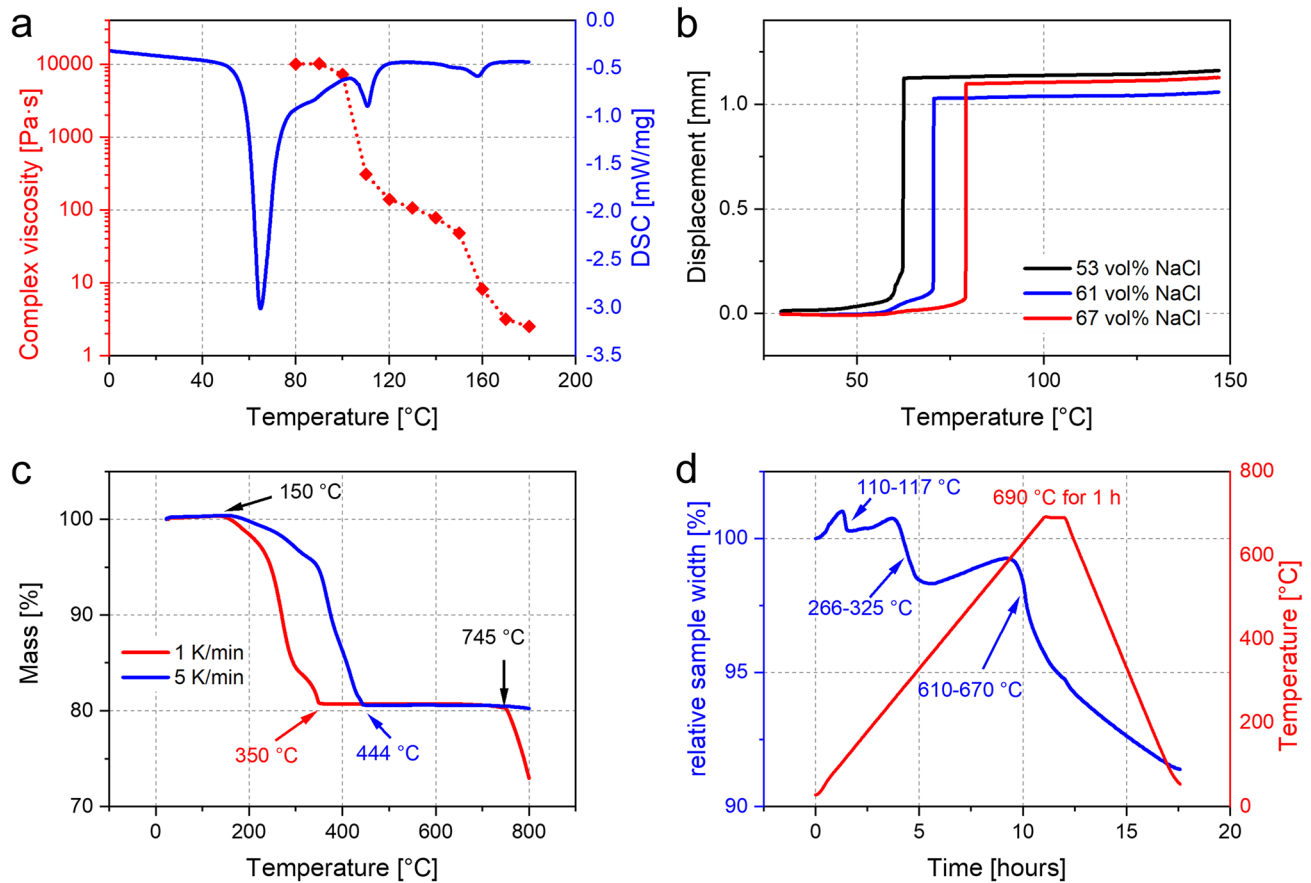
Fig. 1 **a** Rheology (31 rad/s, 0.1% deformation) and DSC measurements of the Embemould binder. **b** Penetration test on feedstocks with different NaCl contents. **c** TGA measurements at different heating rates of a feedstock containing 67 vol% NaCl. **d** Dilatometry on a 3D printed sample with a heat rate of 1 °C/min. A and B adapted from Ref. [28]

body strength. TGA measurements revealed that binder decomposition started at 150 °C therefore setting the upper limit for nozzle temperature during 3D printing (Fig. 1C). The temperature required to achieve full removal of the binder was strongly dependent on the heating rate. With slow heat rates of 1 °C/min samples were fully debound at 350 °C, while that temperature increased to 444 °C with 5 °C/min. The same TGA curves revealed that NaCl started to evaporate at 745 °C. Therefore, 745 °C was the upper limit for NaCl sintering and metal casting. Shrinkage of the 3D printed samples during debinding and sintering was determined by optical dilatometry (Fig. 1D) and is discussed below.

Preliminary extrusion experiments on the 3D printer showed constant filament extrusion between 110 and 140 °C (Fig. 2A). In this temperature range the viscosity is ideal according to rheological measurements. Printing parameters were then optimized on test geometries such as pyramids and cubes (Fig. 2B, C). Satisfactory printing qualities were achieved at printing speeds between 10 and 20 mm/s. Particularly in combination with large nozzles (0.8 mm), the

small diameter of the extrusion screw in the print head was limiting the printing speed to < 20 mm/s, since material extrusion was inconsistent at higher speeds. Therefore, faster printing with large nozzles would require a larger extrusion screw in the print head and a more powerful motor. Most part geometries were printed reliably with two perimeters and a rectangular infill of 50% with lines at + 45° and – 45° printed in every layer. Printing bed adhesion worked well with PEI (polyetherimide) surface at 70 °C to make use of the slight stickiness of the feedstock above 65 °C, the melting temperature of the first binder component. On the other hand, samples easily came off the printing bed at temperatures below 60 °C. Nozzle diameters of 0.4, 0.6, and 0.8 mm and corresponding layer heights of 0.2, 0.3, and 0.4 mm lead to good printing quality in terms of layer-to-layer adhesion and uniform width of the extruded filament (Fig. 2D–F). With the 0.2 mm nozzle, the filament was not extruded homogeneously, since the NaCl particles were too large in relation to the nozzle diameter. For printing with the 0.2 mm nozzle, the feedstock should be prepared with NaCl particle size below 50 μm. Light microscopy and SEM of
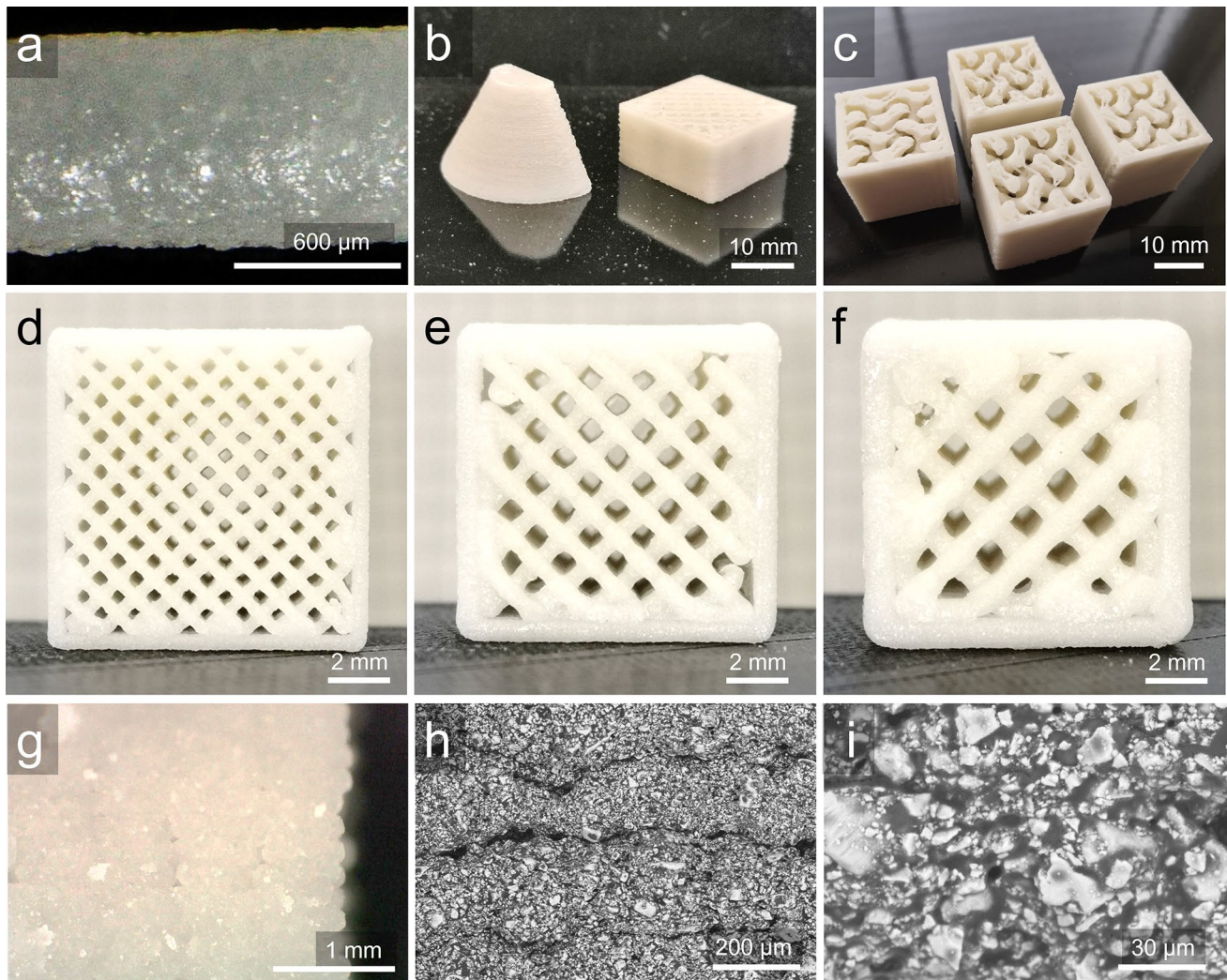
Fig. 2 a Filament extruded from 0.6 mm printer nozzle. **b**, **c** examples of test geometries. D-E: 12×12×12 mm cubes printed with 1 perimeter and 50% rectilinear infill with 0.4 mm nozzle and 0.2 mm layer height (**d**), 0.6 mm nozzle and 0.3 mm layer height (**e**), 0.8 mm nozzle and 0.4 mm layer height (**f**). **g** Light microscope image of a cross-section of a sample printed with 0.6 mm nozzle. H, I: SEM images of the surface of a printed sample showing NaCl crystals (white) embedded in organic binder (gray)

the surface as well as cross-section of green bodies showed a good layer adhesion and high packing density of the printed lines. Furthermore, the NaCl particles were homogeneously distributed in the binder matrix (Fig. 2G–I).

The temperature program for debinding printed samples was chosen according to the sample geometry/size and especially the wall thickness. For samples such as the ones shown in Fig. 2 a heat ramp of 1 °C/min up to 500 °C led to defect-free samples with uniform shrinkage. For larger samples such as the metal casting molds shown below, the temperature was increased more slowly, either 20 or 30 °C/h. The shrinkage of samples during debinding and sintering was observed by optical dilatometry (Fig. 1D). A first shrinkage by roughly 1% occurred at 110 °C when the second component of the binder melted according

to DSC. This shrinkage is reversible since a reversible phase transition is responsible for it and not the irreversible removal/decomposition of a certain component of the sample. A possible consequence of this shrinkage might be mechanical stresses in the printed part as the extruded filament expands slightly when it is deposited on the colder already printed part. Nevertheless, we have not observed any failures in printing which could be attributed to filament expansion during cool down from nozzle temperature (typically 130 °C) to printing bed temperature (70 or 90 °C). A second shrinkage by 2–3% takes place at around 300 °C, in the temperature range where a large fraction of the binder decomposes or evaporates. The main shrinkage by roughly 5% occurs during sintering at 610–690 °C.
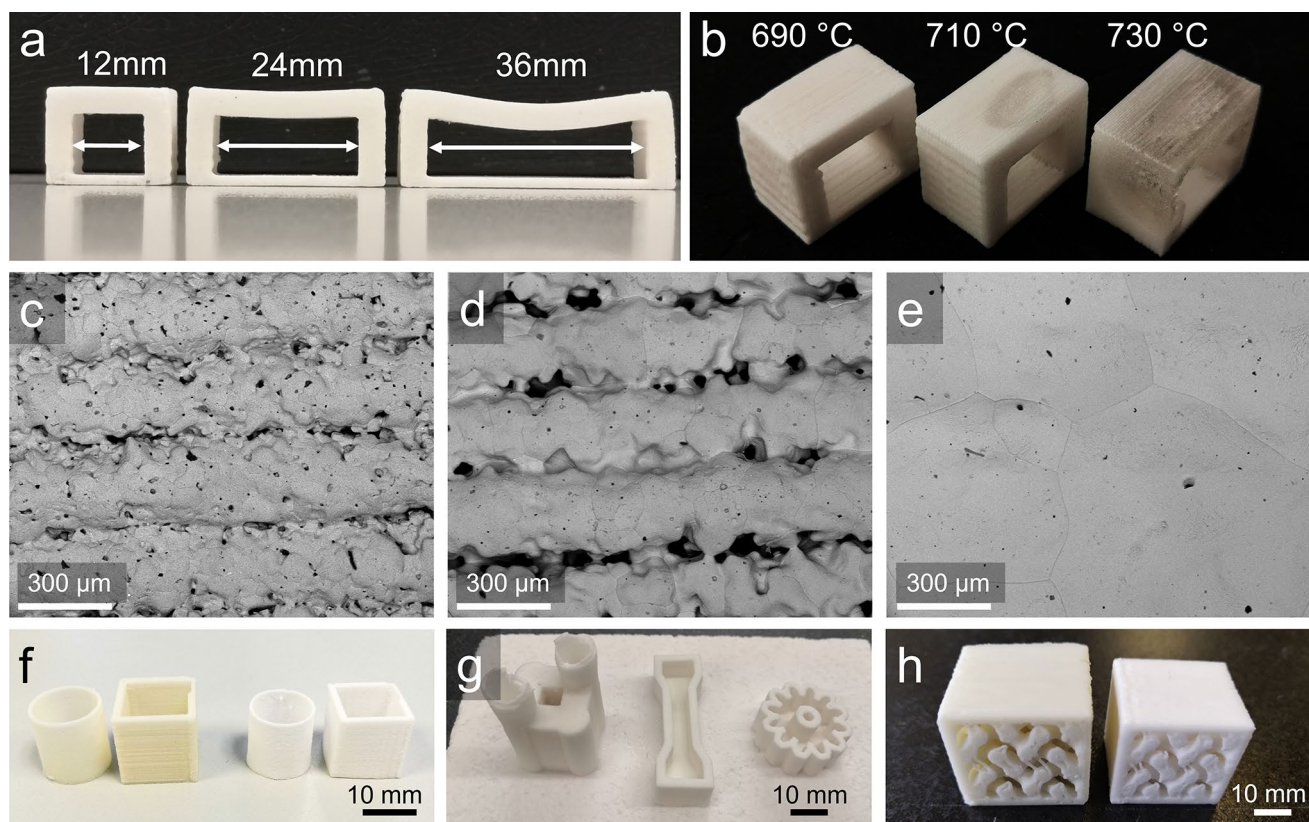
Fig. 3 **a** Sagging experiment for bridges with different lengths sintered at 690 °C. **b** NaCl samples sintered at different temperatures. C-E: SEM images of the surface of samples sintered at 690 °C (**c**), 710 °C (**d**) and 730 °C (**e**). **F** Simple cylinder and cube samples before and after sintering at 690 °C. **g** Different NaCl molds after sintering. **h** Gyroid mold before and after sintering

The sagging behavior of 3D printed parts during sintering was tested with bridge structures of different sizes (12, 24, 36 mm in length, 12 mm width, 12 mm height, Fig. 3A). Upon sintering at 690 °C for 1 h, the 12 mm bridge did not show any sagging, 0.5 mm of sagging was observed for the 24 mm bridge and 3.0 mm for the 36 mm bridge. Therefore, larger overhangs should be avoided, while smaller overhangs of < 12 mm are not expected to lead to deformation during sintering. Alternatively, the sagging should be compensated in the design of the mold when large overhangs are inevitable. Furthermore, different sintering temperatures of 690, 710, and 730 °C were tested and the shrinkage was 9.8% in all cases (Fig. 3B). According to Goodall et al., the main densifying sintering takes place between 620 and 680 °C [31]. At higher temperatures, no more densification was reported, but different sintering mechanisms become dominant, leading to non-uniform shrinkage and deformed samples [31]. SEM images revealed a high porosity of the samples sintered at 690 °C (Fig. 3C). Pores occurred between the layers but also within printing lines. While porosity negatively affects the strength of the samples the pores were too small for metal penetration during casting. At 710 °C, NaCl grains as well as pores grew substantially larger and at

730 °C grains became so large that layers from 3D printing are merged completely, but larger holes formed in the sample due to evaporation–condensation mechanism becoming dominant (Fig. 3D, E) [31, 32]. Some comparisons of parts before and after sintering are shown in Fig. 3F–H.

In an attempt to smoothen the surface of the NaCl molds and therefore increase the surface quality of the molded metal parts, freshly printed as well as sintered NaCl samples were dipped into saturated aqueous NaCl solution for 4–5 min. Figure 4A shows the surface of a reference part which did not undergo any post-treatment and was sintered directly after printing. The layers from printing can easily be distinguished and numerous pores in the range of 5–40 μm are spread all over the surface and arose from the broad and uncontrolled particle size distribution of the NaCl powder used for feedstock production. While the line pattern was transmitted to the casted metal part, the pores were too small to be penetrated by the liquid metal and therefore did not impede the casting. On the contrary, pores of 5–50 μm might improve the casting by acting as vents through which trapped air escapes the NaCl mold. Sintered NaCl samples which were dipped in NaCl solution, dried and sintered again showed an improved surface quality with far fewer
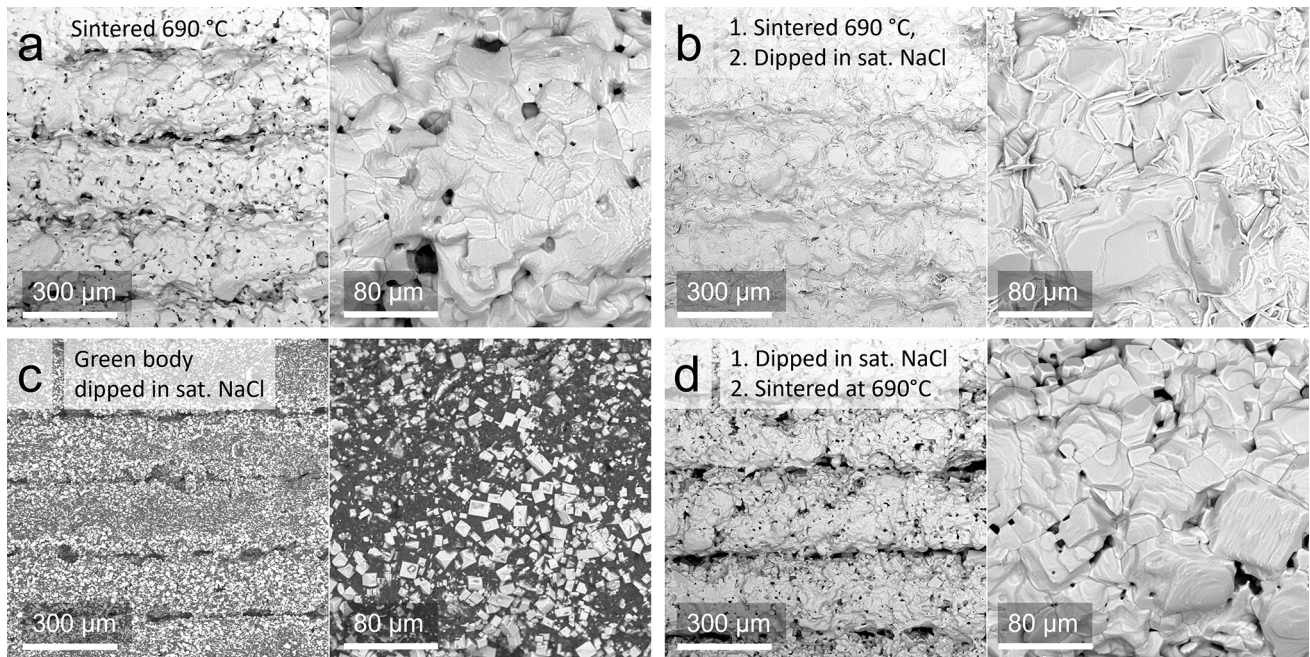
Fig. 4 SEM surface images. **a** Part sintered directly after printing. **b** Part sintered after printing and then dipped into sat. NaCl solution. **c** Printed part dipped in sat. NaCl solution without sintering. **d** Sintered sample which was dipped in sat. NaCl before sintering

pores and smoothened gaps between the printing layers (Fig. 4B). However, soaking sintered NaCl samples in saturated NaCl solution made them very brittle and difficult to handle. Alternatively, printed green bodies were immersed in NaCl solution before sintering. This treatment led to the crystallization of NaCl cubes on the exposed surface of the sample without filling the hidden pores and gaps (Fig. 4C). Consequently, after sintering those samples did not show a

smoother surface or fewer pores as compared to the samples without post-treatment (Fig. 4D).

As a proof of concept to demonstrate the possibility of easy transfer to industrial mass production of molds and cores, NaCl bending test rods were injection molded from the same feedstock used for 3D printing (Fig. 5). SEM investigations of injection molded green bodies showed that the NaCl particles of up to 100 µm particle size were homogeneously encapsulated in the organic binder. During sintering
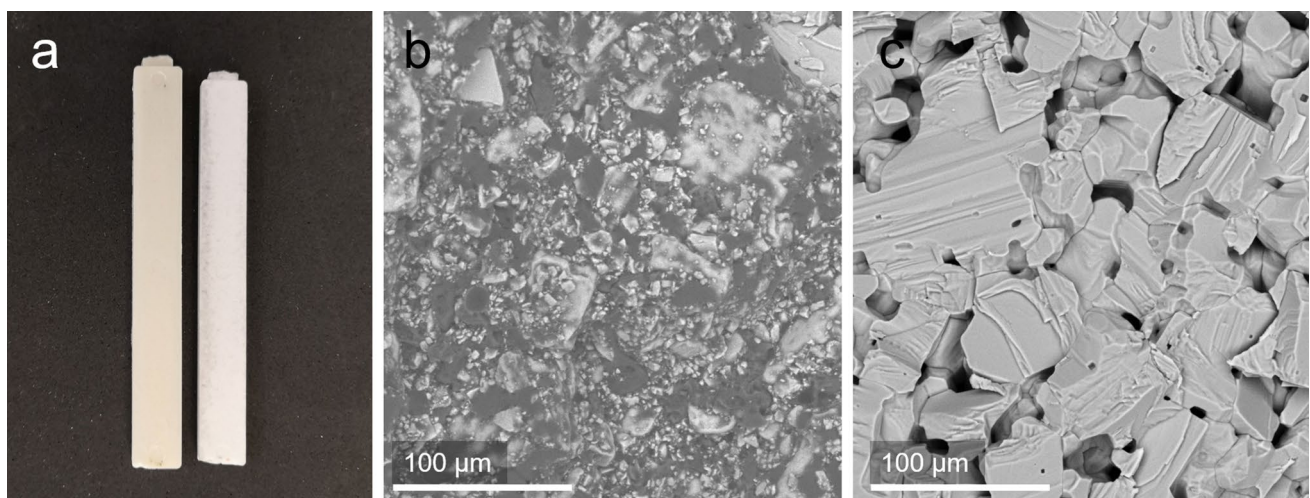

Fig. 5 **a** Photography of injection molded test bars in the green state (left) and after sintering (right). The length of the bar before sintering is 80 mm. **b** SEM of the cross section of an injection molded bar showing NaCl particles in white encapsulated by the binder in dark gray. **c** SEM after sintering showing pure NaCl

the NaCl particles grew significantly with some particles reaching 200–300 μm. This grain growth was not linked to further densification since the dominant densification mechanism at temperatures above 680 °C is evaporation–condensation as suggested by Goodall et al. [31]. Therefore, even higher temperatures or longer sintering times did not decrease the porosity of the parts. Future research should focus on achieving higher density and fewer pores for example by using hot pressing instead of pressure less sintering, the addition of a substance acting as sinter aid or using smaller NaCl particles with a narrower particle size range, but fewer pores will result in a slower dissolution of the salt core after die casting.

The strength of 3D printed NaCl rods with and without post-treatment and injection molded test bars was measured by three point bending tests on sintered samples. Surprisingly, the untreated samples showed the highest bending strength (12 MPa, Fig. 6), despite the samples dipped in NaCl solution after sintering having a much smoother surface with less gaps and pores. Those samples had an average strength of 9 MPa, while the samples dipped in NaCl before sintering had a strength of 10 MPa. As mentioned above, immersing printed and sintered samples in aqueous solutions made them very brittle and apparently the full strength of the part did not reemerge after complete drying and not even after an additional sintering step. The second sintering did indeed increase the bending strength of the samples by 1–1.5 MPa, but similarly so for the untreated parts, which after two rounds of sintering features the highest strength of 13 MPa. The second sintering step did not result in additional shrinkage and densification. Hence, the increased strength is expected to result from improved connectivity
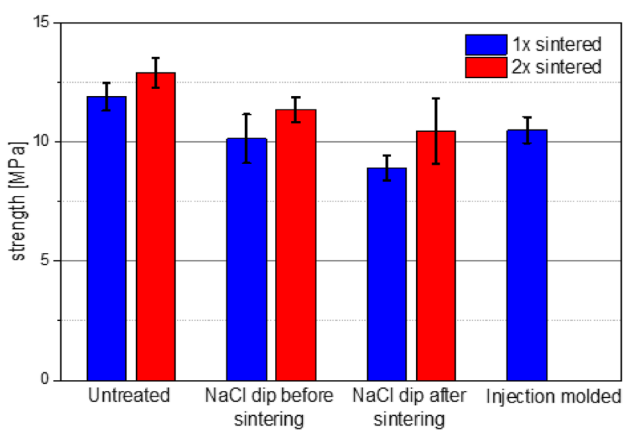

Fig. 6 Three point bending strength of 3D printed and injection molded NaCl specimens. From left to right: untreated samples were sintered once or twice without any treatment after sintering; samples dipped in saturated NaCl solution after printing and then sintered once or twice; samples dipped in saturated NaCl solution after the first sintering; injection molded and sintered parts

between NaCl particles as the NaCl particles grow during sintering. The strength of injection molded samples is similar to 3D printed samples at 10.5 MPa, but the bending strength of all 3D printed samples is much higher than reported for NaCl samples fabricated by casting of molten NaCl (6.7 MPa [33], 5 MPa [4] or pressing of moist NaCl powder (2.3 MPa [5]) For salt cores used in aluminum die casting, even higher bending strengths can be achieved by adding Na_2CO_3[4] or Na_2SO_4 [8, 33] to the NaCl. Alternatively, different sintering processes (hot pressing, vacuum sintering) or smaller NaCl particle sizes could further improve the bending strength.

It is worth mentioning that all 3D printed salt parts presented herein exceed the strength requirements for pressureless or low-pressure aluminum casting, since the sand cores used for those application typically feature bending strengths of only 2–7 MPa [34, 35].

Metal casting was first tested with soldering tin because of its low melting temperature (217 °C) and therefore easier handling as compared to aluminum. Examples of molds as well as the resulting tin parts are shown in Fig. 7. The NaCl mold was heated to 250 °C in a furnace, while the tin was molten in an Al_2O_3 crucible by a hot air gun set to 400 °C and cast into the hot mold. After cooling down, the mold was dissolved under running water or in a water bath in a few seconds or few minutes, depending on the geometry of the casted part. The tin parts manufactured using this method exhibit wall thicknesses as low as 1 mm, for instance in the case of the turbine blades.

Aluminum parts with complex geometry such as gyroid structures could be used for lightweight support structures or heat exchangers due to their favorable mechanical and thermal properties [36, 37]. We chose a gyroid cylinder with 36 mm in diameter and 36 mm in height as a demonstrator object for aluminum casting (Fig. 8). The NaCl mold was designed with thicker external walls (2 mm) as compared to the molds for tin casting, since pressure had to be applied during Al casting. To prepare the casting, both the NaCl mold and Al metal were preheated to 710 °C. Subsequently, the molten metal was poured into the mold and an Al_2O_3 piston was used to apply pressure and ensure complete filling of the mold. Without the application of external pressure, the surface tension of the molten Al prevented it from penetrating the finer structures of the mold, resulting in incomplete filling. After cooling down, the mold was dissolved in a water bath within two minutes revealing the aluminum gyroid structure. 3D printing layers were clearly visible on the cast sample since the mold did not undergo NaCl immersion treatment after sintering. The wall thickness of the structure of 3 mm lies within the range of common wall thicknesses for industrial die casting (approx. 3–11 mm [38, 39]). The part serves as a proof of concept for die casting into MEX printed NaCl molds. However, especially for die
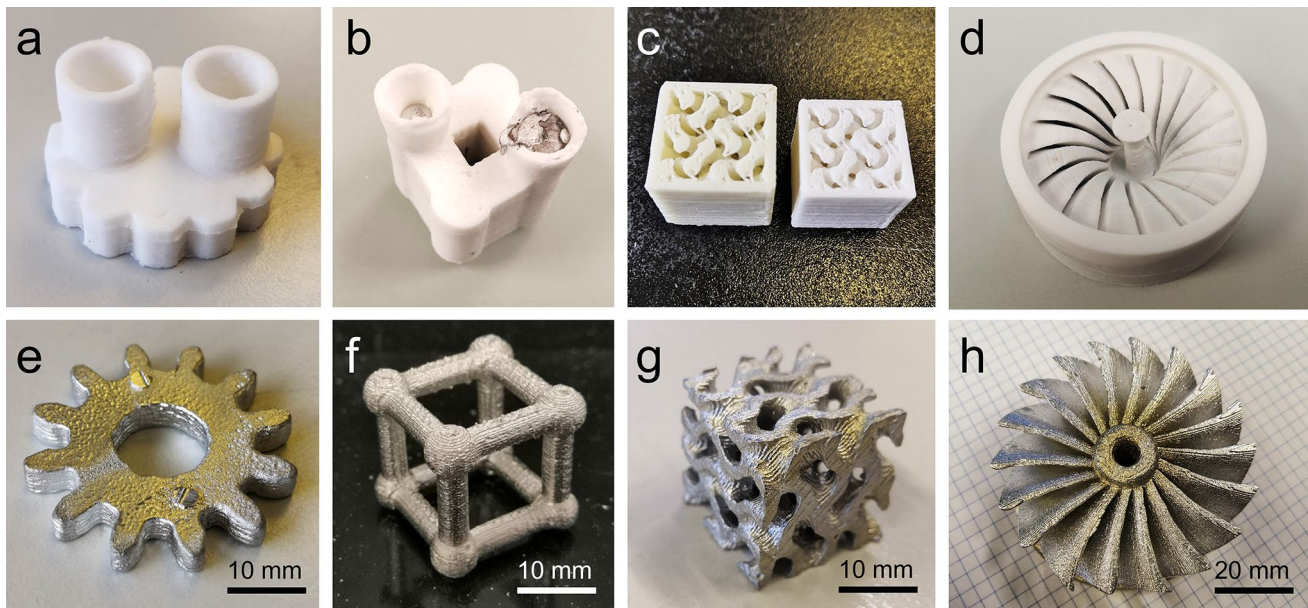
Fig. 7 NaCl molds and corresponding tin parts after dissolution of the mold of increasing complexity: **a**, **e** gear, **b**, **f** cubane, **c**, **g** gyroid cube, **d**, **h** turbine wheel

casting at high pressures, the strength of pure NaCl samples as presented here is likely not sufficient. Feedstocks with NaCl mixed with other salt or ceramics as reinforcements could solve this limitation [6, 8].

4 Conclusion

The 3D printing of sacrificial metal casting molds by material extrusion is a promising approach for producing molds that can accommodate complex geometries such as undercuts and branched cavities. The feedstock presented in this work is prepared from a commercial CIM binder filled with NaCl. After sintering, the mold consists of pure NaCl, which dissolves in water within seconds or few minutes after metal casting. Demonstrator parts such as gear wheels, gyroid structures, and turbine wheels have been successfully cast from tin and aluminum using these molds. The surface of the NaCl molds can be smoothened by immersion of the sintered mold into a saturated NaCl solution. Besides 3D printing, bending test bars were injection molded with the same feedstock. Three-point bending tests showed a high strength of 12–13 MPa for 3D printed and sintered NaCl samples. To enhance the strength of the NaCl molds and enable their use in aluminum die casting, it is possible to reinforce the NaCl with other salts or ceramics. This could also increase the melting temperature, thereby making it possible to cast a wider range of metals with this method.

Fig. 8 **a** NaCl gyroid molds after printing. **b** Sintered NaCl mold cooling down after aluminum casting. The mold was embedded in Al_2O_3 powder and in a larger Al_2O_3 crucible. **c** Aluminum gyroid part after dissolution of the mold
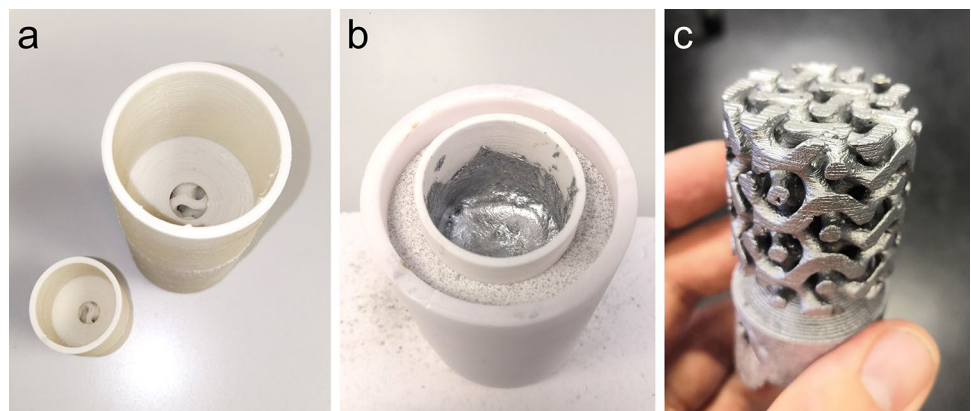
Data availability The data presented in this study are available on request from the corresponding author.

Declarations

Conflict of interest On behalf of all authors, the corresponding author states that there is no conflict of interest.

References

1. Bonollo F, Gramegna N, Timelli G (2015) High-pressure die-casting: contradictions and challenges. Jom 67:901–908. https://doi.org/10.1007/s11837-015-1333-8
2. Collot J (2001) Review of new process technologies in the aluminum die-casting industry. Mater Manuf Process 16:595–617. https://doi.org/10.1081/AMP-100108624
3. Lothar Kallien A (2016) Salzkerne im Druckguss Giesserei 13:2–13
4. Yaokawa J, Miura D, Anzai K et al (2007) Strength of salt core composed of alkali carbonate and alkali chloride mixtures made by casting technique. Mater Trans 48:1034–1041. https://doi.org/10.2320/matertrans.48.1034
5. Beňo J, Adámková E, Mikšovský F, Jelìnek P (2015) Development of composite salt cores for foundry applications. Mater Tehnol 49:619–623. https://doi.org/10.17222/mit.2013.160
6. Xiao Z, Harper LT, Kennedy AR, Warrior NA (2017) A water-soluble core material for manufacturing hollow composite sections. Compos Struct 182:380–390. https://doi.org/10.1016/j.compstruct.2017.09.058
7. Kleger N, Cihova M, Masania K et al (2019) 3D printing of salt as a template for magnesium with structured porosity. Adv Mater. https://doi.org/10.1002/adma.201903783
8. Gong X, Liu X, Chen Z et al (2022) 3D printing of high-strength water-soluble salt cores via material extrusion. Int J Adv Manuf Technol 118:2993–3003. https://doi.org/10.1007/s00170-021-08131-x
9. Kleger N, Fehlmann S, Lee SS et al (2022) Light-based printing of leachable salt molds for facile shaping of complex structures. Adv Mater 34:2203878. https://doi.org/10.1002/adma.202203878
10. Gallien F, Gass V, Mortensen A (2022) Investment casting of periodic aluminum cellular structures using slurry-cast table salt moulds. Mater Des 215:110488. https://doi.org/10.1016/j.matdes.2022.110488
11. Wick-Joliat R, Tschamper M, Kontic R, Penner D (2021) Water-soluble sacrificial 3D printed molds for fast prototyping in ceramic injection molding. Addit Manuf 48:102408. https://doi.org/10.1016/j.addma.2021.102408
12. Basso A, Mendez Ribo M, Halina Danielak A, et al (2019) 3d printed mold for powder injection molding process. In: Proc Jt Spec Interes Gr Meet between euspen ASPE Adv Precis Addit Manuf 71–74
13. Sharifi E, Chaudhuri A, Wæhrens BV et al (2020) Part selection for freeform injection molding: framework for development of a unique methodology. In: Lalic B, Majstorovic V, Marjanovic U et al (eds) Advances in production management systems. Towards smart and digital manufacturing. Springer International Publishing, Cham, pp 723–730
14. Sharifi E, Chaudhuri A, Waehrens BV et al (2021) Assessing the suitability of freeform injection molding for low volume injection molded parts: a design science approach. Sustainability 13:1313. https://doi.org/10.3390/su13031313
15. La Gala A, Ceretti DVA, Fiorio R et al (2022) Comparing pellet- and filament-based additive manufacturing with conventional processing for ABS and PLA parts. J Appl Polym Sci. https://doi.org/10.1002/app.53089
16. Shaik YP, Schuster J, Shaik A (2021) A Scientific Review on Various Pellet Extruders Used in 3D Printing FDM Processes. OALib 08:1–19. https://doi.org/10.4236/oalib.1107698
17. Moreno Nieto D, Molina SI (2020) Large-format fused deposition additive manufacturing: a review. Rapid Prototyp J 26:793–799. https://doi.org/10.1108/RPJ-05-2018-0126
18. Pignatelli F, Percoco G (2022) An application- and market-oriented review on large format additive manufacturing, focusing on polymer pellet-based 3D printing. Prog Addit Manuf 7:1363–1377. https://doi.org/10.1007/s40964-022-00309-3
19. Nötzel D, Eickhoff R, Hanemann T (2018) Fused filament fabrication of small ceramic components. Materials (Basel) 11:1463. https://doi.org/10.3390/ma11081463
20. Orlovská M, Chlup Z, Bača Ľ et al (2020) Fracture and mechanical properties of lightweight alumina ceramics prepared by fused filament fabrication. J Eur Ceram Soc 40:4837–4843. https://doi.org/10.1016/j.jeurceramsoc.2020.02.026
21. Lengauer W, Duretek I, Fürst M et al (2019) Fabrication and properties of extrusion-based 3D-printed hardmetal and cermet components. Int J Refract Met Hard Mater 82:141–149. https://doi.org/10.1016/j.ijrmhm.2019.04.011
22. Abel J, Scheithauer U, Janics T et al (2019) Fused filament fabrication (FFF) of metal-ceramic components. J Vis Exp 2019:1–13. https://doi.org/10.3791/57693
23. Hadian A, Koch L, Koberg P et al (2021) Material extrusion based additive manufacturing of large zirconia structures using filaments with ethylene vinyl acetate based binder composition. Addit Manuf 47:102227. https://doi.org/10.1016/j.addma.2021.102227
24. Hadian A, Fricke M, Liersch A, Clemens F (2022) Material extrusion additive manufacturing of zirconia parts using powder injection molding feedstock compositions. Addit Manuf 57:102966. https://doi.org/10.1016/j.addma.2022.102966
25. He Q, Jiang J, Yang X et al (2021) Additive manufacturing of dense zirconia ceramics by fused deposition modeling via screw extrusion. J Eur Ceram Soc 41:1033–1040. https://doi.org/10.1016/j.jeurceramsoc.2020.09.018
26. Shen T, Xiong H, Li Z et al (2021) Fused deposition fabrication of high-quality zirconia ceramics using granular feedstock.

Ceram Int 47:34352–34360. https://doi.org/10.1016/j.ceramint.2021.08.348

27. Cano S, Gonzalez-Gutierrez J, Sapkota J et al (2019) Additive manufacturing of zirconia parts by fused filament fabrication and solvent debinding: Selection of binder formulation. Addit Manuf 26:117–128. https://doi.org/10.1016/j.addma.2019.01.001

28. Wick-Joliat R, Penner D (2023) Flexible interconnected ceramic parts 3D printed by two-component material extrusion with water-soluble support structures. J Eur Ceram Soc. https://doi.org/10.1016/j.jeurceramsoc.2023.03.069

29. Wick-Joliat R, Schroffenegger M, Penner D (2023) Multi-material ceramic material extrusion 3D printing with granulated injection molding feedstocks. Ceram Int 49:6361–6367. https://doi.org/10.1016/j.ceramint.2022.10.170

30. Wick-Joliat R, Mauchle S, Kontic R et al (2021) MoSi2/Al2O3/feldspar composites for injection-molded ceramic heating elements. Adv Eng Mater 23:2100517. https://doi.org/10.1002/adem.202100517

31. Goodall R, Despois J-F, Mortensen A (2006) Sintering of NaCl powder: mechanisms and first stage kinetics. J Eur Ceram Soc 26:3487–3497. https://doi.org/10.1016/j.jeurceramsoc.2005.12.020

32. Ashby MF (1974) A first report on sintering diagrams. Acta Metall 22:275–289. https://doi.org/10.1016/0001-6160(74)90167-9

33. Wang X, Liu W, Liu X, Song L (2023) First-principles calculation and mechanical properties of NaCl–Na2SO4 composite water-soluble salt core. Int J Met 17:263–271. https://doi.org/10.1007/s40962-022-00769-x

34. Stauder BJ, Kerber H, Schumacher P (2016) Foundry sand core property assessment by 3-point bending test evaluation. J Mater Process Technol 237:188–196. https://doi.org/10.1016/j.jmatprotec.2016.06.010

35. Zhao D, Guo W, Zhang B, Gao F (2019) Investigation on moist silica sand's circulation for sand mold printing with line-forming. Rapid Prototyp J 25:1411–1420. https://doi.org/10.1108/RPJ-05-2018-0113

36. Caiazzo F, Alfieri V, Guillen DG, Fabbricatore A (2022) Metal functionally graded gyroids: additive manufacturing, mechanical properties, and simulation. Int J Adv Manuf Technol 123:2501–2518. https://doi.org/10.1007/s00170-022-10334-9

37. Li X, Xiao L, Song W (2021) Compressive behavior of selective laser melting printed Gyroid structures under dynamic loading. Addit Manuf 46:102054. https://doi.org/10.1016/j.addma.2021.102054

38. Qi M, Li J, Kang Y (2019) Correlation between segregation behavior and wall thickness in a rheological high pressure die-casting AC46000 aluminum alloy. J Mater Res Technol 8:3565–3579. https://doi.org/10.1016/j.jmrt.2019.03.016

39. Kowalczyk W, Dańko R, Górny M et al (2022) Influence of high-pressure die casting parameters on the cooling rate and the structure of EN-AC 46000 Alloy. Materials (Basel) 15:5702. https://doi.org/10.3390/ma15165702

Publisher's Note Springer Nature remains neutral with regard to jurisdictional claims in published maps and institutional affiliations.